PAPER • **OPEN ACCESS**

Comparison of two UHPFRC premixes blast resistance with the commonly used concrete based on the failure mode prediction

To cite this article: O Janota *et al* 2019 *IOP Conf. Ser.: Mater. Sci. Eng.* **596** 012017

IOP Conf. Series: Materials Science and Engineering **596** (2019) 012017 doi:10.1088/1757-899X/596/1/012017

Comparison of two UHPFRC premixes blast resistance with the commonly used concrete based on the failure mode prediction

O Janota[1], E Bonnet[2] and M Foglar[1]

[1] Faculty of Civil Engineering, Czech Technical University in Prague, Thákurova 7/2077, 166 29 Prague 6, Czech Republic
[2] R&D Lafargeholcim, 95 rue du Montmurier, Saint Quentin Fallavier, France

E mail: ondrej.janota@fsv.cvut.cz

Abstract. This paper presents results of extensive experimental programme which took place in 2019. Two proprietary ultra-high performance fibre reinforced composite materials were tested for their blast (contact and close-in) resistance. In total, twenty-eight specimens were tested. Specimens were loaded with explosive charge of weight of 100 - 1000 g in various distances. All specimens were visually evaluated for the damage extend, failure mode and crack pattern. Results from the experiment were compared to the results available in literature for normal strength reinforced concrete. Results showed that both tested premixes performed better than ordinary mixtures in terms of blast resistance. Difference between tested materials and commonly used mixture are described as well. Finally, both materials were compared from the material properties point of view as well as by their blast resistance performance.

1. Experimental program

Experimental program took place at the fields of the University of Pardubice in 2018. Twenty–eight specimens with dimensions 1000 x 1000 mm and three thicknesses (100; 150 and 200 mm) were tested. For manipulation with the specimen, four handlings were placed at the contact side in each corner and two handlings were placed at the side edge. For the selection of the dimensions two criteria were considered [1]. Primary, the dimensions were set by the numerical simulation which confirmed that the pressure wave reached the bottom surface before the reflection from the side edges occurred. Secondly, the manipulation with the specimen was considered.

Blast load was created by the explosive charge of SEMTEX 1A. The weight of the explosive (0 – 1000 g) as well as the distance (0 – 100 mm) between the explosive and top surface varied. Therefore, both types of blast load, contact and close-in blast, were performed. Shape of the explosive charges was cylinder with length/diameter ration equal to one. Detonation point was set approximately 20 mm under the top edge of each explosive charge.

Each specimen was put on steel frame (Fig. 1). Therefore, the specimen can be considered as a slab simply supported along all four edges. Height of the steel frame was set 720 mm and it served as a place for a mirror which enabled the recording of the bottom surface needed to be placed under the specimen. Reflection of the pressure wave from the ground was prevented by the elevation of the specimen [2] [3]. Each shot was recorded by two high-speed cameras. For experiment scheme see Fig. 2.

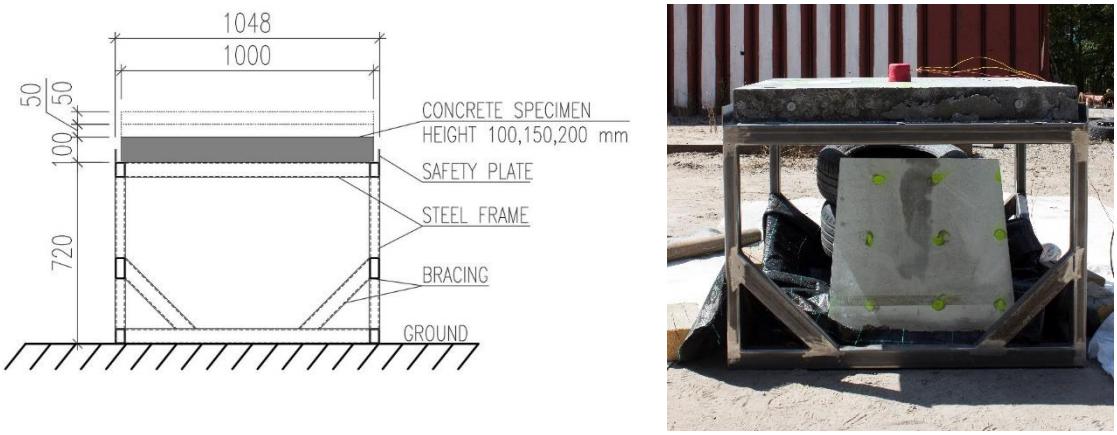

Figure 1. Left – cross section of the specimen supported by the steel frame; Right – specimen with the explosive charge.

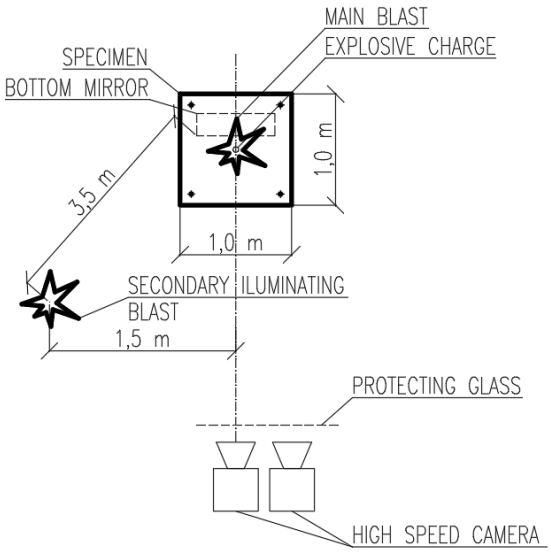

Figure 2. Scheme of the experiment site.

2. Material properties

Two proprietary UHPFRC materials with compressive strength higher than 150 MPa were tested during this experimental program. First material was Premix A with compressive strength 180 MPa, second material was Premix B with compressive strength 150 MPa. Amount of fibres in each material, their length and yield strength were similar in both premixes. Both materials were tested on three specimens for their compressive and tensile strength and flexural energy. Tensile strength and flexural energy were calculated from the results of the four-point bending tests (Tab. 1). Compressive strength was calculated from the compressive test (Tab. 2). Results of the tests are presented in the Fig. 3 and 4.

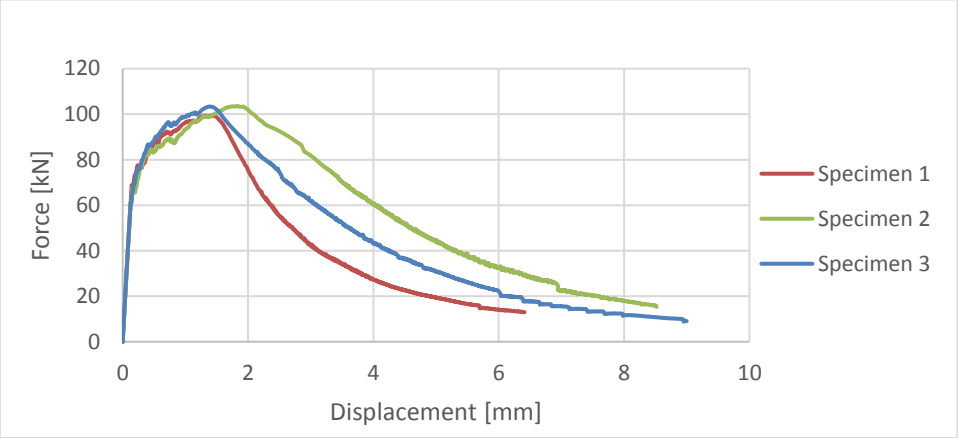

Figure 3. Four-point bending test of premix A.

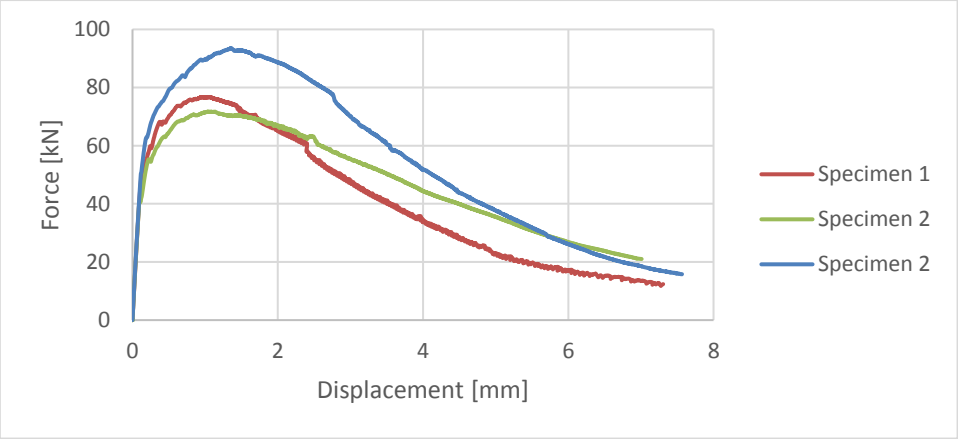

Figure. 4. Four-point bending test of premix B.

Table 1. Material properties of both premixes – four-point bending test.

Premix A								
Spec. Nr [-]	**Spec. length [mm]**	**Spec. width [mm]**	**Spec. height [mm]**	**Spec. weight [kg]**	**Density [kg/m^3]**	**Max. force [kN]**	**Ten. Strength [MPa]**	**Flex. energy [MJ]**
1	700	151.4	149.9	39.1	2460	99.48	17.4	13.7
2	700	151.1	148.2	39.0	2488	103.58l	18.4	21.7
3	700	150.7	150.5	39.1	2464	103.34l	18.1	18.2
Average value	**-**	**-**	**-**	**-**	**2471**	**102.13**	**18.0**	**17.9**
Premix A								
Spec. Nr [-]	**Spec. Nr [mm]**	**Spec. Nr [mm]**	**Spec. Nr [mm]**	**Spec. Nr [kg]**	**Spec. Nr [kg/m^3]**	**Spec. Nr [kN]**	**Spec. Nr [MPa]**	**Spec. Nr [MJ]**
1	700	151.4	151.0	39.5	2483	76.76	13.5	13.4
2	700	151.3	148.3	39.4	2524	71.78l	12.9	14.9
3	700	150.9	148.2	39.9	2551	93.58l	16.6	18.4
Average value	**-**	**-**	**-**	**-**	**2519**	**80.71**	**14.3**	**15.5**

Table 2. Material properties of both premixes – compressive test.

Spec. Nr	Spec. length	Spec. width	Max. force	Comp. strength
[-]	**[mm]**	**[mm]**	**[kN]**	**[Mpa]**
1-1	150	150	3476.0	154.5
1-2	150	150	3875.0	172.2
2-1	150	150	4108.0	182.6
2-2	150	150	3934.0	174.8
3-1	150	150	3630.0	161.3
3-2	150	150	3613.0	160.6
Average value	**-**	**-**	**3773.0**	**166.7-**
Spec. Nr	**Spec. Nr**	**Spec. Nr**	**Spec. Nr**	**Spec. Nr**
[-]	**[mm]**	**[mm]**	**[kN]**	**[Mpa]**
1-1	150	150	2985.0	132.7
1-2	150	150	3426.0	152.3
2-1	150	150	3552.0	157.9
2-2	150	150	3535.0	157.1
3-1	150	150	3577.0	159.0
3-2	150	150	3671.0	163.1
Average value	**-**	**-**	**3458.0**	**153.7**

3. Experimental results

The evaluation of the results presented in this paper is based mainly on the visual inspection and damage measurements. Fundamental damage parameters (damage depth, damage size, failure mode and shape) were measured for the evaluation of the empirical prediction which were derived for concrete specimens by McVay [4] and Morishita [5], [6]. Both approaches are based on the following parameters:

- Scaled thickness ($T/W^{1/3}$) – thickness of the specimen (T) divided by the weight of the explosive (W).
- Scaled distance ($R/W^{1/3}$) – distance between detonation point and top surface of specimen (R) divided by the weight of the explosive (W).
- Scaled damage ($C_D + S_D)/T$ – Summation of damage depth of soffit and contact side ($C_D + S_D$) divided by the thickness of the specimen (T).
- Failure mode – type of the final damage; generally, three types are considered in literature (Fig. 5).

Based on huge amount of experimental results and above-mentioned parameters, McVay derived empirical approach for the prediction of the result. However, these prediction curves were derived for the normal strength and reinforced concrete. As there are the differences in the material properties between normal strength concrete and UHPFRC, the validation of this approach needed to be done. Moreover, the superior blast resistance of UHPFRC to normal strength concrete can be proven with this approach. Morishita's [5], [6] approach, which is more recent, was based on the calculation of the scaled damage based on the scaled thickness. This approach was also derived for the normal strength reinforced concrete.

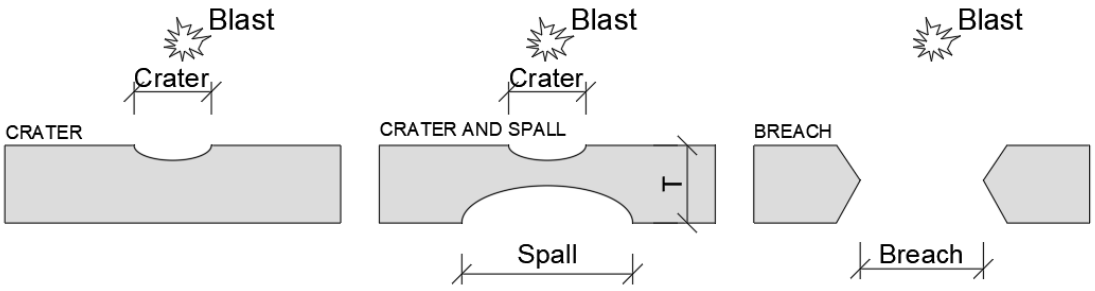

Figure. 5. Failure modes – Left – Crater; Middle – Crater and Spall; Right – Breach.

One of the experiment targets was to describe the boundaries between different failure modes. Seventeen of the specimens ended with crater and spall failure mode. Three of the specimens ended with only spall damage. Five specimens ended with only crater or no damage failure mode and six were breached. Overview of the parameters of each shot and reached failure mode is presented in Tab. 3.

Table 3. List of experiment dispositions and final failure mode for each specimen.

Shot number	Premix	Spec. thick.	Exp. weight	Exp. length	Distance	Failure mode	Scaled distance
[-]	[-]	[mm]	[g]	[mm]	[mm]	[-]	[m/kg$^{1/3}$]
1	A	100	400	61	0	Breach	0.051
2	A	100	200	58	0	Crater and spall	0.060
3	A	150	400	66	0	Crater and spall	0.057
4	A	100	400	74	100	No damage	0.192
5	A	100	1000	90	60	Crater and spall	0.119
6	A	100	400	60	10	Crater and spall	0.062
7	A	100	200	58	0	Crater and spall	0.060
8	A	200	1000	95	20	Crater and spall	0.087
9	B	100	400	700	100	Spall	0.187
10	A	100	400	700	100	Spall	0.187
11	A	100	400	700	100	No damage	0.187
12	A	100	400	700	0	Breach	0.062
13	A	100	400	60	0	Breach	0.050
14	A	150	1000	96	0	Breach	0.070
15	A	200	1000	90	30	Crater and spall	0.092
16	A	100	200	55	25	Crater and spall	0.094
17	B	100	300	70	100	Crater and spall	0.205
18	B	100	300	70	0	Crater and spall	0.068
19	B	200	500	75	0	Crater and spall	0.063
20	B	100	1000	80	60	Breach	0.110
21	B	100	200	50	100	Spall	0.204
22	B	100	150	45	25	Crater and spall	0.086
23	B	150	500	75	40	Crater and spall	0.110
24	B	100	500	75	20	Breach	0.087
25	B	100	100	47	25	Crater	0.103
26	B	150	400	64	30	Crater	0.092
27	B	100	800	76	60	Crater and spall	0.114
28	B	200	300	50	0	Crater	0.041

3.1. Crack pattern

Two types of crack systems were observed. Firstly, the radial cracks appeared on most of the specimens. These cracks were wider; mostly starting on the border of damage zone and propagating in all directions. However, mostly in the direction towards the edge with side handlings. Moreover, on some of these specimens one main radial crack penetrated fully to the opposite surface. These cracks occurred on all of the specimens damaged by the breach and on the most of the specimens damaged by the crater and spall.

Second type of cracks was thin peripheral cracks appearing mostly on contact surface and in some cases on soffit. These peripheral cracks were observed on specimens with all three failure modes, mostly on the contact side. On some specimens these cracks were continuously joined into a circle (Fig. 6). However, peripheral cracks were thin and did not propagate deeper into the specimen which was in contrary to some of the radial cracks that propagated through the specimen thickness.

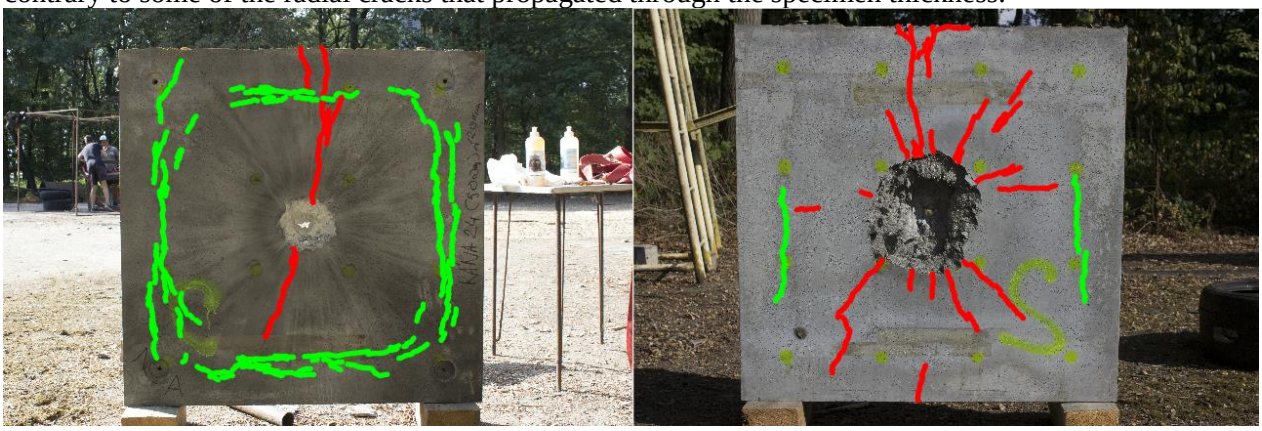

Figure 6. Cracks patterns, red – radial cracks, green – peripheral cracks.

3.2. Multiple wave reflection

Spalling of the debris on the soffit revealed multiple wave reflections as the pressure wave reached the interface between concrete and the air. Concrete spall created new interface for the still propagating pressure wave. This multiple wave reflection shaped probably spall contours. If there was only one reflection, the damaged surface was smooth. Once the multiple reflection occurred, surface was more rugged and not so continuous as in the case with only one reflection, see Fig.7.

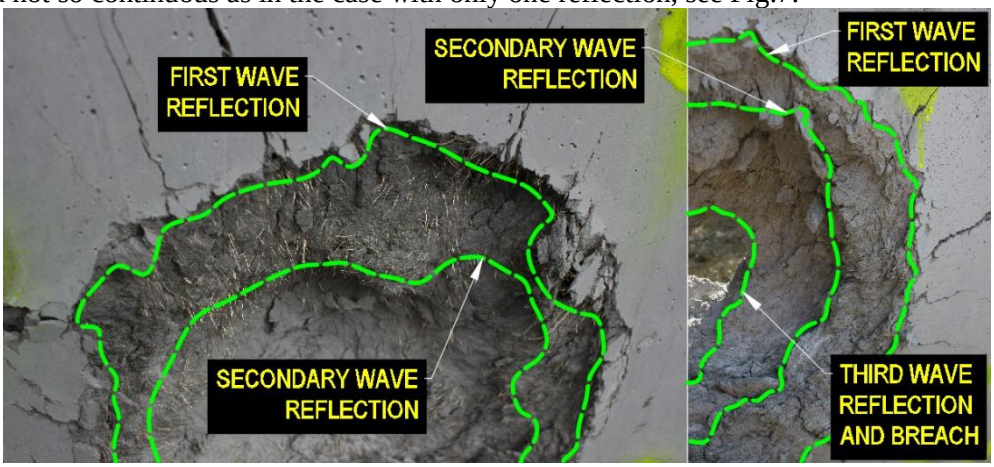

Figure 7. Damage areas with traces obvious for multiple reflection of pressure wave.

4. Empirical approach to the failure mode estimation for the UHPFRC

4.1. McVay approach to failure mode prediction

Although, the experiment covered only a part of the McVay's graph and for better specification of the boundary curves and their mathematical description more experiments are needed, twenty-eight specimens and their failure modes provided good opportunity for the comparison of the initially derived results with the results of UHPFRC material. Results indicates (Fig. 8) that originally derived boundaries are not fully valid for the UHPFRC material. Crater or no damage and breach failure modes clearly defined both boundaries. Even some results which were classified as crater and spall and lay near the boundary between no damage and crater and spall were threshold spall. Both curves defining boundary

between the failure modes were shifted downward. Inclination of both curves stayed similar. This indicates that UHPFRC material is more blast resistant than the normal strength concrete and more energy needs to be produced to reach spall or breach failure mode.

Both materials behaved very similar but slight difference was observed. Specimens made of Premix B were more likely breached with the lower scaled distance. This difference was probably caused by the difference of the material properties. As the results were located only in part of the McVay's graph, the difference between both materials would be covered by the statistical dispersion with increase of the results.

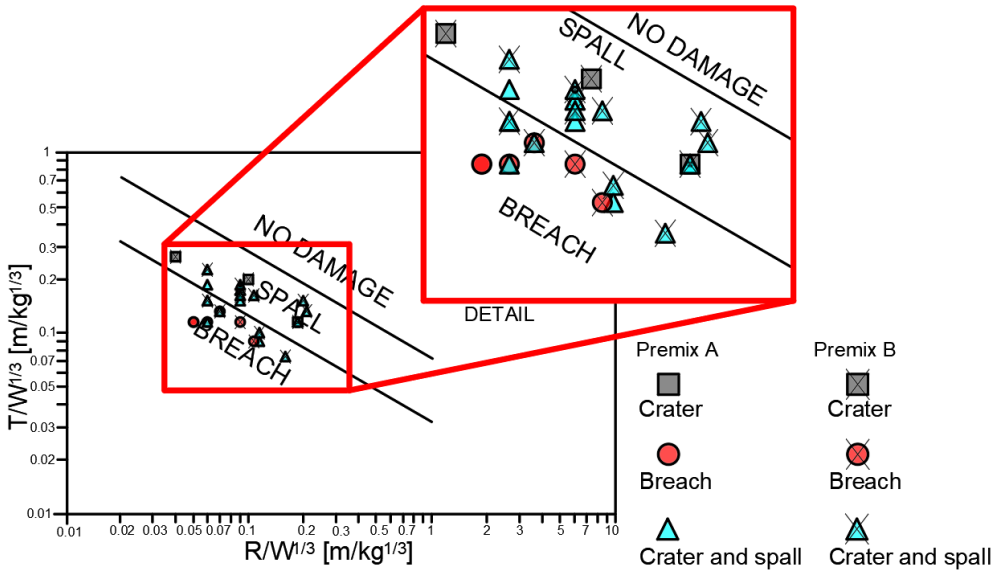

Figure 8. Comparison of the experimental results with the failure mode prediction derived by McVay.

4.2. Morishita approach to failure mode prediction

Morishita's approach was initially derived for the contact blast. Therefore, only scaled thickness was considered. It is important to emphasize that not all specimens were loaded by contact blast. Therefore, the results compared to Morishita's approach can be distorted by this fact. When applying the Morishita's [2] [3] equations for different failure modes on the tested UHPFRC material, it is obvious that limits (2.0 for breach, 3.6 for crater and spall) changed.

Results presented in Fig. 9 clearly showed new limits for failure modes. Limit value of scaled thickness for boundary between crater/no damage and crater and spall was set 2.1 cm/g$^{1/3}$. Boundary between crater and spall and breach failure mode was set 1.3 cm/g$^{1/3}$. Moreover, these limits also indicate that inclination of the crater and spall damage depth prediction curve is steeper than the original Morishita's curve and boundaries for this type of failure are closer to each other. This phenomenon is in agreement with the results from the McVay's approach.

As the previously described approach did not consider influence of the explosive distance from the specimen top surface, dependency of the scaled damage on the scaled distance is presented in Fig. 10. Results indicates that if the scaled distance is 1.0 cm/g$^{1/3}$ or less the damage depth is 40% of the specimen thickness or more. On the other side, specimens with scaled distance 1.5 – 2.0 cm/g$^{1/3}$ ended with damage depth lesser than 40% of the specimen thickness. Range of scaled distance between 1.1 and 1.5 cm/g$^{1/3}$ cannot be described for lack of experiments. Results of specimens with crater and spall indicates direct ration between damage depth and scaled distance.

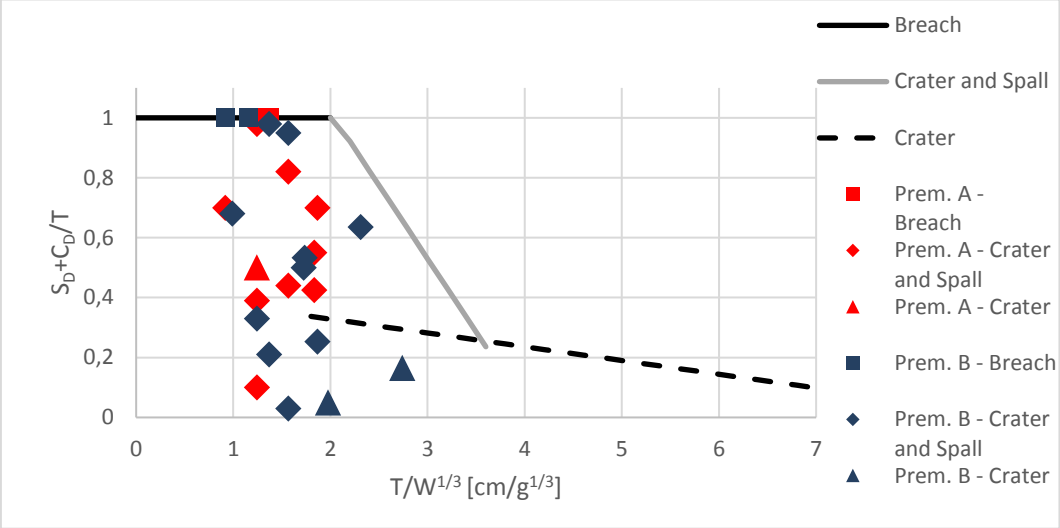

Figure 9. Comparison of the experimental results with the failure mode prediction derived by Morishita.

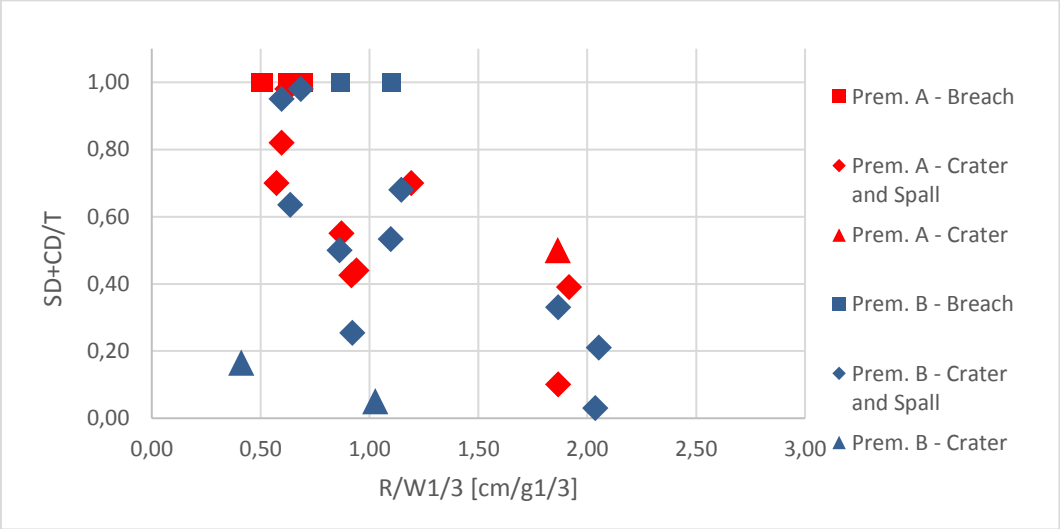

Figure 10. Development of the scaled damage and its dependency on the scalded distance.

As in the McVay's approach both materials were compared to each other (Fig. 11). Premix A with the better material properties performed better. The difference between two materials for the tested scaled distances varied from 10 % to 20 % of the specimen thickness. The difference between both materials was more obvious for lower values of the scaled distance. With the increase of scaled distance, the difference decreased. Regression analysis performed on the results for each material revealed that the dependency of the scaled damage on the scaled distance can be described by the exponential function. However, R-value which describes strength of the linear analysis was relatively low. Results from the Morishita's approach are in agreement with the results from McVay's approach.

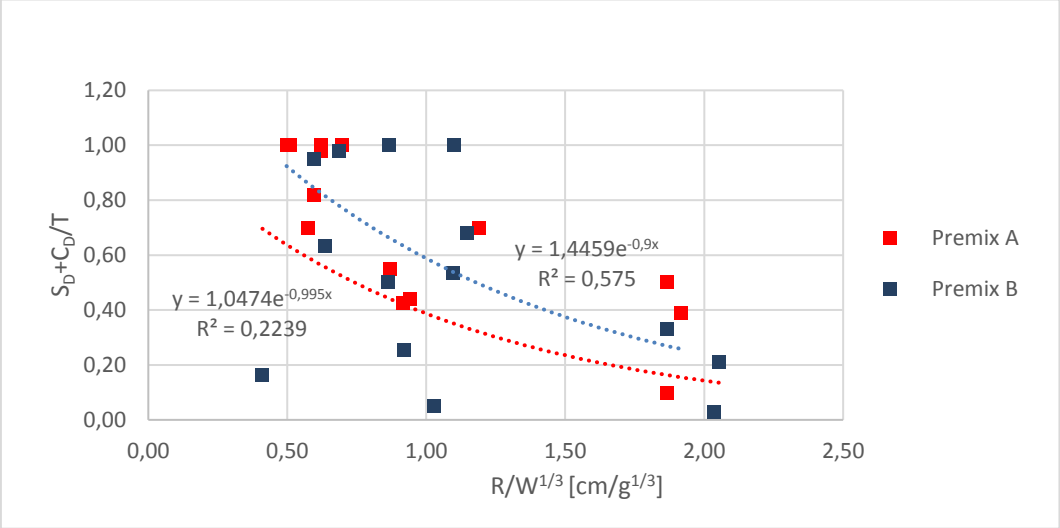

Figure 11. Regression analysis for damage prediction.

5. Conclusion

This paper presented results from the experiment focused on the blast resistance of UHPFRC slabs. Two materials with compressive strength 150 MPa and 180 MPa were tested for contact and close-in blast resistance. Altogether, twenty-eight specimens were tested, fourteen specimens for each material. Specimens' dimensions were 1000 x 1000 mm with thicknesses of 100, 150 and 200 mm. Each specimen was tested for different explosive weight and scaled distance. Results presented in this paper were based on the visual evaluation of the experiment results. Firstly, the damage extend, depth and failure mode were observed and measured. Then the results were compared to McVay's and Morishitas's approaches for the prediction of the blast performance of concrete specimens.

One of the experiment targets was to set boundary curves between different failure modes for UHPFRC material. Most specimens ended with crater and spall failure mode and the extent of damage on the soffit was slightly higher than on the contact side.

Visual observations revealed two different systems of cracks on both surfaces. First system was represented by radial cracks which were observed on most of the specimens. Second system of cracks consisted of peripheral cracks which were mostly located at the specimen edges. Radial cracks were relatively wide, and in some cases propagated through the thickness of the specimen. Contrary to radial cracks, peripheral cracks were located only at the contact and soffit surfaces and did not propagate into the specimens.

Comparison of experiment results to the empirical approaches derived by McVay and Morishita revealed superior behaviour of UHPFRC to concrete with normal strength. Both boundaries between different failure modes were clearly defined and shifted towards lower numbers of scaled thickness/distance. Comparison of both approaches revealed that both approaches were in agreement. Substitution of scaled thickness with scaled distance revealed clear influence of this factor. With the increasing scaled distance by two or four times, the total damage depth decreases up to 20% of the initial value.

Both materials were compared to each other as well. Comparison revealed similar blast resistance of both materials. However, the premix A performed slightly better than premix B. This was caused by the better material properties of Premix A. The difference was not clearly set, and it is probable that if the number of specimens increased, the difference would be dissolved into the statistical dispersion.

Acknowledgements
This work was financially supported by Grant Agency of the Czech Republic, project no. 17-23067S, which is gratefully acknowledged.

References

[1] Kovar M, Foglar M and Hajek R 2014. *The blast performance of real-scale reinforced concrete specimens with varying fiber types and content. Structures Under Shock and Impact XIII*, pp 159-169.
[2] Foglar M, Pachman J, Pelikan V, Hájek R, Künzel M and Kovář M 2014 *The structural response of a reinforced concrete specimen subjected to adjacent blast loading*, pp. 171-179.
[3] Foglar M, Hajek R, Fladr J, Pachman J and Stoller J 2017. *Full-scale experimental testing of the blast resistance of HPFRC and UHPFRC bridge decks. Construction and Building Materials*, 145, pp.588-601.
[4] McVay M 1988. *Spall damage of concrete structures.*
[5] Morishita M, Tanaka H, Ando T and Hagiya H 2004. *Effects of Concrete Strength and Reinforcing Clear Distance on the Damage of Reinforced Concrete Slabs Subjected to Contact Detonations. Concrete Research and Technology*, 15(2), pp.89-98.
[6] Morishita M, Tanaka H, Ito T and Yamaguchi H 2000. *Damage of Reinforced Concrete Slabs Subjected to Contact Detonations. Journal of Structural Engineering*, Vol.46A, pp.1787-1797, (in Japanese)